Since January 2020 Elsevier has created a COVID-19 resource centre with free information in English and Mandarin on the novel coronavirus COVID-19. The COVID-19 resource centre is hosted on Elsevier Connect, the company's public news and information website.

blood advances

American Society of Hematology
2021 L Street NW, Suite 900,
Washington, DC 20036
Phone: 202-776-0544 | Fax 202-776-0545
bloodadvances@hematology.org

Lymphatic coagulation and neutrophil extracellular traps in lung-draining lymph nodes of COVID-19 decedents

Tracking no: ADV-2022-007798R2

Margo Macdonald (Pritzker School for Molecular Engineering, United States) Rachel Weathered (University of Chicago, United States) Emma Stewart (Pritzker School for Molecular Engineering, United States) Alexandra Magold (University of Chicago, United States) Anish Mukherje (University of Chicago, United States) Sandeep Gurbuxani (University of Chicago, United States) Heather Smith (University of Chicago, United States) Phillip McMullen (University of Chicago, United States) Jeffrey Mueller (University of Chicago, United States) Aliya Husain (The University of Chicago, United States) Calixto Mateos Salles (University of Chicago, United States) Priscilla Briquez (Universitats Klinikum Freiburg, Germany) Sherin Rouhani (University of Chicago Medicine, United States) Jovian Yu (University of Chicago, United States) Jonathan Trujillo (University of Chicago, United States) Athalia Pyzer (University of Chicago Medicine, United States) Thomas Gajewski (University of Chicago, United States) Anne Sperling (University of Virginia, United States) Witold Kilarski (University of Chicago, United States) Melody Swartz (Ben May Department of Cancer Research, United States)

Abstract:
Clinical manifestations of severe COVID-19 include coagulopathies that are exacerbated by the formation of neutrophil extracellular traps (NETs). Here, we report that pulmonary lymphatic vessels, which traffic neutrophils and other immune cells to the lung-draining lymph node (LDLN), can also be blocked by fibrin clots in severe COVID-19. Immunostained tissue sections from COVID-19 decedents revealed widespread lymphatic clotting not only in the lung, but notably in the LDLN, where the extent of clotting correlated with the presence of abnormal, regressed, or missing germinal centers. it strongly correlated with the presence of intralymphatic NETs. In mice, TNFα induced intralymphatic fibrin clots, and this could be inhibited by DNAse 1, which degrades NETs. In vitro, TNF induced lymphatic endothelial cell upregulation of ICAM-1 and CXCL8 among other neutrophil-recruiting factors as well as thrombomodulin downregulation. Furthermore, in decedents, lymphatic clotting in LDLNs. In a separate cohort of hospitalized patients, serum levels of MPO-DNA (a NET marker) inversely correlated with antiviral antibody titers, but D-dimer levels, indicative of blood thrombosis, did not correlate with either. In fact, patients with high MPO-DNA but low D-dimer levels generated poor anti-viral antibody titers. This study introduces lymphatic coagulation in lungs and LDLNs as a clinical manifestation of severe COVID-19 and suggests the involvement of NETosis of lymphatic-trafficking neutrophils. It further suggests that lymphatic clotting may correlate with impaired formation or maintenance of germinal centers necessary for robust antiviral antibody responses, although further studies are needed to determine whether and how lymphatic coagulation impacts adaptive immune responses.

Conflict of interest: No COI declared

COI notes: The authors declare no competing financial interests.

Preprint server: No;

Author contributions and disclosures: MAS, MEM and WWK were responsible for overall study conceptualization and design. AIS, SG, PM, ANH, JM and HS planned and carried out the autopsy tissue collection and pathological analysis, including GC analysis by SG. AIM, AM, CMS, MEM, ECS, RKW, PB, WWK, and MAS conducted experiments and analyzed data. AIS provided control tissue and serum samples. SJR, JV, JT, and ARP, and TFG planned and carried out the collection of patient serum samples, clinical data, and D-dimer analysis shown in Fig. 6 and 6S. The manuscript was written by MEM, MAS, ECS, CMS, and WWK. MEM and MAS acquired funding for the project and MAS was responsible for overall study supervision.

Non-author contributions and disclosures: No;

Agreement to Share Publication-Related Data and Data Sharing Statement: Emails to the corresponding author

Clinical trial registration information (if any):

Title: Lymphatic coagulation and neutrophil extracellular traps in lung-draining lymph nodes of COVID-19 decedents

Authors: Margo E. MacDonald[1,5], Rachel K. Weathered[1], Emma C. Stewart[1,2], Alexandra I. Magold[1], Anish Mukherjee[1], Sandeep Gurbuxani[6], Heather Smith[6], Phillip McMullen[6], Jeffrey Mueller[6], Aliya N. Husain[6], Calixto M. Salles[1], Priscilla Briquez[1,8], Sherin J. Rouhani[4], Jovian Yu[4], Jonathan Trujillo[4], Athalia R. Pyzer[4] Thomas F. Gajewski[2-4], Anne I. Sperling[2,3], Witold W. Kilarski[1], and Melody A. Swartz[1-3]

Affiliations:

[1]Pritzker School for Molecular Engineering, University of Chicago, Chicago, IL, USA

[2]Committee on Immunology, University of Chicago, Chicago, IL, USA

[3]Ben May Department of Cancer Research, University of Chicago, IL, USA

[4]Department of Medicine, University of Chicago, Chicago, IL, USA

[5]Biophysical Sciences Program, University of Chicago, Chicago, IL, USA

[6]Department of Pathology, University of Chicago, Chicago, IL, USA

Correspondence: Melody A. Swartz, University of Chicago, melodyswartz@uchicago.edu

Contact the corresponding author for data sharing: melodyswartz@uchicago.edu.

Abstract

Clinical manifestations of severe COVID-19 include coagulopathies that are exacerbated by the formation of neutrophil extracellular traps (NETs). Here, we report that pulmonary lymphatic vessels, which traffic neutrophils and other immune cells to the lung-draining lymph node (LDLN), can also be blocked by fibrin clots in severe COVID-19. Immunostained tissue sections from COVID-19 decedents revealed widespread lymphatic clotting not only in the lung, but notably in the LDLN, where the extent of clotting correlated with the presence of abnormal, regressed, or missing germinal centers. it strongly correlated with the presence of intralymphatic NETs. In mice, TNFα induced intralymphatic fibrin clots, and this could be inhibited by DNAse 1, which degrades NETs. *In vitro*, TNFα induced lymphatic endothelial cell upregulation of ICAM-1 and CXCL8 among other neutrophil-recruiting factors as well as thrombomodulin downregulation. Furthermore, in decedents, lymphatic clotting in LDLNs. In a separate cohort of hospitalized patients, serum levels of MPO-DNA (a NET marker) inversely correlated with antiviral antibody titers, but D-dimer levels, indicative of blood thrombosis, did not correlate with either. In fact, patients with high MPO-DNA but low D-dimer levels generated poor anti-viral antibody titers. This study introduces lymphatic coagulation in lungs and LDLNs as a clinical manifestation of severe COVID-19 and suggests the involvement of NETosis of lymphatic-trafficking neutrophils. It further suggests that lymphatic clotting may correlate with impaired formation or maintenance of germinal centers necessary for robust antiviral antibody responses, although further studies are needed to determine whether and how lymphatic coagulation impacts adaptive immune responses.

Key points

Lymphatic clotting in lung-draining lymph nodes of COVID-19 decedents correlate with intralymphatic NETosis

Patients with severe COVID-19 with low antiviral antibody titers have high serum levels of NETosis biomarkers

Introduction

SARS-CoV-2 infection has caused over 6 million deaths worldwide[1], from respiratory failure, septic shock, multi-organ failure, and other consequences of severe pulmonary infection[2]. Coagulopathies are among the most widely reported clinical correlates of disease severity and include venous and arterial thromboses, microvascular occlusions, disseminated intravascular coagulation, and bleeding disorders[3,4]; approximately 20-50% of hospitalized COVID-19 patients exhibit blood coagulation test abnormalities, including elevated D-dimer levels, thrombocytopenia, and prolonged prothrombin time[5,6]. In addition to these standard indicators of coagulation, elevated serum levels of neutrophil extracellular trap (NET) markers have also been reported in hospitalized COVID-19 patients[6–8], and both NET levels and elevated circulating neutrophil-to-lymphocyte ratios were among the first reported predictors of disease severity[9–11]. Intravascular NETs form when neutrophils adhere to and become activated by injured endothelium, expelling their DNA into large 'nets' that trap platelets to initiate clot formation and inhibit fibrinolysis, activate factor XII, and induce DNA-mediated thrombin generation to further promote coagulation[6,12,13]. Immunothromboses containing NETs have been observed in blood vessels in COVID-19 autopsy sections[14].

Fibrin clots can also occur in lymphatic vessels, and have been reported in lymphedema, lymphatic filariasis, lymphangiectasia, and cancer[15,16], although experimental studies are scarce. In general, lymph coagulates slower than blood, consistent with the lack of platelets, lower levels of Factors VIII and V, and higher levels of fibrinolytic factors[15]. However, neutrophils can enter inflamed lymphatic vessels and migrate to the draining lymph nodes[17–24], with their entry and migration facilitated by lymphatic endothelial cells (LECs) that upregulate adhesion molecules

and secrete neutrophil chemoattractants like CXCL8 when inflamed[17,19,20]. LECs may also activate neutrophils to form NETs since CXCL8 is a potent driver of NETosis[25,26].

Considering that NETs contain extracellular DNA, histones, and tissue factor[12] that may initiate coagulation in the absence of platelets, we hypothesized that lymphatic clotting is a clinical feature of severe COVID-19 disease and is promoted by lymphatic-associated NETosis. If so, this may have particular significance because a subset of severe COVID-19 patients have been reported to exhibit an impaired adaptive immune response, marked by regressed germinal centers (GCs) and extrafollicular B cell activation[27–29]. Transport of immune cells and viral antigens to the LN is a key step in the adaptive immune response, and blockages in lymphatic vessels may therefore impair downstream aspects of adaptive immunity including GC formation and antibody production.

Here, we examined the relationship between NETs, lymphatic vessels, and fibrin coagulation in severe COVID-19 using autopsy sections of lung and lung-draining lymph node (LDLN). We found widespread fibrin lymphatic clotting that was correlated with both intralymphatic NETs and abnormal GC architecture in LDLNs. LECs in clotted vessels also exhibited downregulated thrombomodulin, which was also downregulated in LECs *in vitro* by TNFα. In a separate cohort of COVID-19 patients, we found an inverse correlation between MPO-DNA, a NETosis marker, and antiviral antibody titers; furthermore, patients who failed to generate antibodies were more likely to have high MPO-DNA. In the ear skin of mice, we could demonstrate that lymphatic clotting could be induced by local injection of TNFα in a NET-dependent manner. Together, these findings suggest that COVID-19-associated coagulation is not limited solely to blood vasculature, but extends to the lymphatic vasculature, where it may be driven by NETs rather than platelet activation. Because lymphatic vessels are responsible for the

transport of antigen and immune cells to the LN and GCs are a key part of the humoral immune response, lymphatic clotting and intralymphatic NETosis may have important consequences relating to antiviral antibody production in patients with severe COVID-19 or other viral infections.

Methods

Standard procedures of cell culture, qPCR, ELISA, and immunostaining are described in the Supplemental Methods.

Human Tissue Procurement

Postmortem tissues from lungs and LDLNs were obtained from 16 patients who died from SARS-CoV-2 infection and 9 control patients who died prior to the pandemic, including 3 who died of H1N1, at the University of Chicago Medical Center (Tables S1-S2). Patient demographics were representative of the patient population at UCMC. All policies were reviewed and approved by UChicago's infection control, and autopsy procedures followed CAP and CDC guidelines[30]. The study was conducted in accordance with the Declaration of Helsinki. Due to metastatic cancer involvement, LDLNs from 3 COVID-19 patients and one control were excluded from analysis. Non-COVID-19 lung controls were obtained from the Gift of Hope Regional Organ Bank of Illinois (ROBI). All tissues were formalin-fixed and paraffin-embedded prior to sectioning.

Serum samples from hospitalized COVID-19 patients were obtained from the UChicago COVID-19 biobank study (IRB 20-0520) as described earlier[31]. Daily SpO2/FiO2 ratios were calculated by averaging all clinical measurements available per patient per day. The lowest daily SpO2/FiO2 ratio during a patient's initial hospitalization was used to assign disease severity.

Quantification of lymphatic clotting, neutrophils, and NETs

To quantify neutrophil and NET density in patient lungs and LDLNs, sections were imaged and analyzed after thresholding using Fiji's particle analyzer plugin. Intralymphatic fibrin and NETs were quantified manually in whole-slide tiled images (20x); each vessel was assigned a clotting score (0=no fibrin, 1=fibrin along the luminal surface only, 2=partially clotted (<10%), 3=partially clotted (>10%), 4=fully clotted) and NET score (0=no NETs, 1=NETs along the lumen only, 2=NETs integrated into clot). Scores for all vessels in each LDLN were averaged to give fibrin clotting and NET scores for each patient.

LN Scoring

Quality of GC structures and overall LN architecture were assessed from slides stained with H&E or immunostained for CD3, CD20, CD83 and GL7. GCs were analyzed by follicle size, ratio of tingible body macrophages (TBM) versus medium- and large-body cells within the follicle, degree of hyalinization, overall LN architecture integrity, and distribution of activated T and B cells. LNs were assigned an H&E score (0=primary follicles only as in a naïve setting, 1=robust GCs, 2=weak GCs, 3=lack of GCs in infection setting, 4=regressed GCs, and 5=no apparent follicles). They were also assigned a lymphocyte distribution score (0=small follicles only with distinct zones, 1=large follicles with distinct zones, 2=mixed follicle size, slight loss of integrity, 3=small follicles only in infection setting, 4=mixed follicle size, moderate loss of integrity, and 5=diffuse B cell zone, complete loss of integrity). Lastly, LNs were assigned a GC activation score (0=predominantly primary follicles, activation markers absent from follicle, naïve setting; 1=predominantly reactive GCs, activation markers present within follicle, either naïve or infection setting; 2=follicular activation with minor abnormalities in follicle structure,

little or no extrafollicular activation; 3=predominantly small primary follicles in infection setting, lack of GC response determined by decreased activation markers; 4=moderate abnormalities in follicle activation pattern (including extensive cell drop-off), can include strong follicle activation with extrafollicular activation; 5=extensive extrafollicular B cell activation, poor overall follicle formation/activation). Scores for each patient were summed to create an overall GC abnormality score.

Animals

All procedures were approved by the University of Chicago (ACUP 72414). C57Bl/6 mice (Jackson Laboratories) were used between 6-10 weeks of age. Intravital immunofluorescence was performed as described previously[32].

In vivo labeling of fibrin

40 ml of 10 mg/ml fibrinogen (F8630-1G; Sigma-Aldrich) in PBS was reacted with 1.6 ml of 4 mg/ml FITC or AF-647 (ThermoFisher Scientific) for 1h. Fibrinogen was dialyzed 4x in 4L PBS. 100µl of labeled fibrinogen was injected intravenously into mouse tail veins 15-30 min after treatment expected to induce intralymphatic coagulation (thrombin or cytokine injection).

Thrombomodulin and NETosis blocking in vivo

Thrombin inactivation was achieved by reacting of thrombin (50 µl of 1 U/µl) with 1 mM p-amidinophenylmethylsulfonyl fluoride (p-APMSF, Millipore Corp.) for 2h. 0.5 µl inactive thrombin was injected i.d., alone or with 10 ng/µl TNFα or 10 µg/µl IL-1β (both from Peprotech)

into the dorsal ear dermis. To degrade NETs, mice were injected i.p. with 500 IU DNAse 1 (Sigma-Aldrich) in 0.5 ml immediately after i.d. injections of TNFα.

Statistics and Reproducibility

All statistical analyses and linear regressions were performed using GraphPad Prism. One-way ANOVA with Tukey multiple comparisons post-test used to determine p values for multiple groups, unless otherwise noted. For comparison between two groups, Mann-Whitney U-tests and Student's t-tests were used as noted in figure legends.

Results

Intralymphatic fibrin clots are prevalent in lungs and LDLNs of COVID-19 decedents

Since pulmonary coagulation is a key clinical feature of severe COVID-19[3,4,6], we first asked whether lymphatic vessels in patient lungs also contained fibrin clots by immunostaining lung tissue sections from 16 COVID-19 decedents (Table S1) and 8 controls (Table S2). As expected, we found abundant evidence of intravascular and interstitial coagulation, and interestingly, many intact lymphatic vessels also contained fibrin clots (Fig. 1). However, the lung lymphatic vessels were frequently severely damaged and interstitial fibrin widespread, precluding meaningful quantification.

Surprisingly, when analyzing the LDLNs, we found more extensive lymphatic clotting within intact lymphatic vessels (Fig. 2A-B), particularly in the subcapsular sinus (Fig. S1). In contrast, fibrin-containing lymphatics were rare in LDLNs of patients who died of causes unrelated to viral infection (Fig. 2C, Table S2). However, in three patients who died of severe H1N1 influenza, lymphatic clotting in the LDLN was similar to the COVID-19 decedents (Fig.

2D). We then analyzed every lymphatic vessel in each tile-scanned LDLN image, assigning each vessel a fibrin score based on the extent of blockage (Fig. 2E). The LDLNs of COVID-19 decedents had higher fractions of lymphatic vessels that were mostly or fully clotted (fibrin score of 3-4) compared to those of controls (Fig. 2F), while both COVID-19 and H1N1 LDLNs had substantially higher fibrin scores than controls (Fig. 2G). This suggests that lymphatic clotting in LDLNs may be a common clinical feature of severe pulmonary viral infection, where clotting in the subcapsular sinus may block lymph entry into the LN.

Lymphatic clotting correlates with abnormal or missing germinal centers in LDLNs

It has been documented that dysregulated adaptive immune responses and impaired GC formation can occur in severe cases of COVID-19[27,28]. Since lymphatic clotting would likely disrupt the entry and exit of fluid, antigens, and APCs to and from the LDLN, we asked whether the lymphatic clotting we observed COVID-19 decedent LDLNs could be correlated to this phenomenon. To test this, we created scoring criteria: (i) "H&E score" for GC architecture, (ii) "GC activation score" based on immunostaining for GL7 (B cell activation marker) and CD83 (light zone marker), (iii) "lymphocyte distribution score" based on staining for B and T cell markers, and (iv) an overall "GC abnormality score" reflecting the sum of (i)-(iii).

By H&E, most LDLNs from COVID-19 decedents, unlike controls, showed regressed GCs and abnormal follicle architecture based on the increased presence of TBMs and lack of a mantle zone (Fig. 3A-B), while H&E scoring showed significant differences among COVID-19 and H1N1 LDLNs compared to controls (Fig. S2A-B). When considering GC activation, COVID-19 LDLNs also exhibited increased extrafollicular activation based on GL7 staining and were more likely to show diffuse regions of B cell activation compared to controls, whose

activation patterns were contained within discrete oval-shaped follicles (Fig. S2C-D). CD83 and GL7 staining overall was decreased within COVID-19 follicles, potentially indicating follicular regression or a failure to develop a strong GC reaction (Fig. 3C). There was a significant difference in the GC activation scores between COVID-19 and control decedents, and between H1N1 and control decedents (Fig. S2C-D). Lastly, we found that while the lymphocyte distribution scores were not significantly different in LDLNs between COVID-19, H1N1 and control groups (Fig. S2E-F), some COVID-19 LDLNs exhibited poor distinctions between B and T cell zones, with diffuse lymphocyte mixing not present in controls (Fig. 3D).

Interestingly, the summed GC abnormality scores showed significant differences between COVID-19 and H1N1 LDLNs compared to controls (Fig. 3E) and positively correlated with the degree of lymphatic clotting in the LDLN (Fig. 3F). Together, these data suggest that fibrin-blocked lymphatics in the LNs may potentially contribute to the abnormal GC architecture observed by us and others in COVID-19, although further experimental studies are necessary to determine causation.

Lymphatic clotting correlates with intralymphatic NETs and downregulated thrombomodulin in the LDLNs of COVID-19 decedents

In blood vessels, NETs contribute to immunothrombosis in COVID-19 through neutrophil-platelet interactions[14]; although platelets are absent in lymph, NETs can also promote clotting in a platelet-independent manner[12]. To gain insight into possible mechanisms of lymphatic clotting, we stained LDLN sections for NETs as well as thrombomodulin, which is known to be downregulated by TNFα in blood vessels to promote clotting there[14]. Interestingly, we found that in fibrin-filled lymphatic vessels, NETs were often incorporated into the fibrin clots (Fig. 4A).

On average, clotted vessels contained more NETs than open or unclotted vessels in COVID-19 LDLNs as well as in control and H1N1 LDLNs (Fig. 4B). In addition, when vessels were scored for NETs (0=no NETs, 1=NETs along lymphatic lumen, 2=NETs incorporated into clot), the average score correlated with the percentage of lymphatics containing clots as well as the GC abnormality score (Fig. 4C-D, Fig. S3).

Interestingly, decedents with higher neutrophil densities in the lung had higher percentages of clotted lymphatic vessels in the LDLN (Fig. 4E-F), while NET counts in the lungs did not correlate with the percentage of clotted lymphatic vessels in the LDLN (Fig. 4G). This suggests that lymphatic clots seen in the LDLN did not originate from dislodged upstream clots in the lung, but rather from neutrophils trafficking out of the lung and NETosing in the LDLN lymphatics. In addition, neutrophil and NET counts were not globally increased in COVID-19 LDLNs compared to controls (Fig. S4) so the correlation between lymphatic clotting and NETs appears to be specific to intralymphatic NETs rather than overall NETs in the LDLN.

We next stained LDLN sections for fibrin, podoplanin and thrombomodulin (Fig. S5A-B). Interestingly, within each tissue, clotted vessels had decreased thrombomodulin expression compared to open vessels (Fig. S5C). This trend was observed within every patient except one (Fig. S5C) and suggests that inflammation-induced downregulation of lymphatic thrombomodulin may contribute to lymphatic clotting.

In vitro, LECs secrete CXCL8, upregulate ICAM-1, and downregulate thrombomodulin in response to TNFα

Because the increased presence of NETs was specific to clotted vessels, we asked whether inflamed LECs may be recruiting neutrophils and inducing NETosis. In culture, LECs

responded to TNFα treatment by increasing their secretion of CXCL8 and expression of ICAM-1 (Fig. S6A-B); these were not affected by IL6 or IFNγ. TNFα also led to increased transcription of the neutrophil chemoattractants CCL2, CCL3 and CCL5 (Fig. S6C) as well as CXCL1, CXCL2 and CXLC3. Interestingly, thrombomodulin mRNA also decreased after treatment with TNFα as well as IL6, GM-CSF, and IFNγ (Fig. S6D). Together, these results suggest that LECs directly respond to inflammatory cytokines associated with COVID-19, especially TNFα, in ways that promote neutrophil attraction, NETosis, and fibrin formation.

High NET levels in patient serum correlate with lower levels of anti-RBD antibody titers

In a separate patient cohort, serum was collected at various timepoints from patients with SARS-CoV-2 infection, while control serum was obtained from non-hypertensive donors prior to the pandemic (Table S4). COVID-19 patients with co-morbidities such as active cancer, organ transplant, or immunosuppression that would impact NET levels or the anti-SARS-CoV-2 antibody response were excluded, as well as patients who had received convalescent plasma.

Using ELISA, we measured levels of the NET marker MPO-DNA and IgG antibody titers against the receptor-binding domain (RBD) of COVID-19's Spike protein. Consistent with other studies, COVID-19 patient serum contained higher levels of MPO-DNA than controls (Fig. 5A); interestingly, these were not correlated with levels of D-dimer, a common marker of blood thrombosis (Fig. 5B). Next, we compared serum MPO-DNA levels with anti-RBD antibody titers and found a significant negative correlation between the two (Fig. 5C). In addition, when categorized by having low (2-4), moderate (4.5-5.5), or high (6-8) anti-RBD titers, the MPO-DNA levels in serum from patients with low anti-RBD titers were significantly higher than those in serum from patients with high anti-RBD titers (Fig. 5D). All patients with low anti-RBD titers

had mid-high levels of serum MPO-DNA (Fig. 5E). When categorized by having low (<0.33), mid (>0.33 and <0.5) or high (>0.5) serum MPO-DNA levels, anti-RBD titers were significantly lower in the high and mid MPO-DNA groups compared to the low MPO-DNA group (Fig. 5F). Interestingly, most patients with high levels of MPO-DNA but low levels of D-dimer had low anti-RBD antibody levels (Fig. 5B-C). All patients with low serum MPO-DNA levels had moderate or high anti-RBD antibody titers, and patients with moderate to high serum MPO-DNA levels had higher proportions of low anti-RBD titers (Fig. 5G). Because there was no correlation between serum MPO-DNA and D-dimer, it's possible that the relationship between MPO-DNA and anti-RBD titers is independent of blood clotting and may be due to lymphatic clotting instead.

While NET levels negatively correlated with anti-RBD titers, there was no significant correlation between NET levels and the SpO2/FiO2 ratio, a marker of disease severity where lower SpO2/FiO2 ratios indicate more severe disease (Fig. S7A). While more patients with mild disease had low NET levels, patients across all severity levels also exhibited mid-high NET levels, and consistent with earlier reports of severe COVID-19 patients[6–8], most patients in our cohort had high NET levels (Fig. S7B,C).

In mice, locally injected TNFα drives NET-dependent lymphatic clotting

Finally, we sought to determine whether lymphatic clotting could be induced in mouse skin. Under steady-state conditions in mouse ear skin, lymphatic endothelium stained strongly for thrombomodulin but not von Willebrand factor relative to blood (Fig. 6A). We then injected TNFα locally in the mouse ear, and using fluorescently labeled fibrinogen injected i.v. to visualize fibrin clot formation, we could observe fibrin clots in lymphatic vessels (Fig. 6B-C).

These clots were mostly found in collecting vessels around junctions and valves. Addition of both TNFα and IL-1β did not increase the extent or kinetics of clotting (Fig. 3C). Clotting in lymphatic collectors could also be induced with i.d. injections of inactivated thrombin, which competitively inhibits thrombomodulin (Fig. 6C). While lymphatic clots were relatively sparse, each mouse (n=9) exhibited some level of lymphatic occlusion, and clot formation was sufficient to prevent lymphatic drainage from lymphatics efferent to clotted collectors (Fig. S8A-B).

To test whether NETs are involved in TNFα-induced lymphatic clotting, we used DNAse 1 (injected i.p.) to degrade NETs immediately after i.d. TNFα injection (Fig. 6D). Whole-mount staining for LYVE-1 and citrullinated histone 3 (H3cit), a specific marker of NETosis, revealed that many of the clots within lymphatic vessels contained NETs (Fig. 6E). Importantly, we found substantially fewer lymphatic clots in the ears of mice that received DNAse 1 (Fig. 6E-F), suggesting that NETs play important roles in TNFα-induced lymphatic clotting.

Discussion

Our findings demonstrate that lymphatic coagulation, particularly in the LDLN, is a clinical feature of fatal COVID-19. Furthermore, we found that fibrin-filled lymphatic vessels were more likely to contain intralymphatic NETs, and lymphatic clotting in the LDLN correlated with abnormal or missing GCs, while serum NET levels negatively correlated with anti-RBD antibody titers. Since elevated NETs and regressed GCs have both been independently reported in severe COVID-19[6–8,27,28], our findings suggest a possible link between the two.

Lymph coagulation was first recognized over a century ago[36–38], yet has received little research attention[15]. It has been described in lymphatic-related diseases[15,39–43], but otherwise,

clinical evidence of pathological lymph clotting is rare. We speculate that this is because the effects of lymphatic clots are likely less detectable, and less acute, than those of blood clots.

When isolated, lymph clots ~2-5x slower than corresponding plasma[15,37,38]. Lymph lacks platelets, and contains lower concentrations of clotting factors and higher levels of fibrinolytic factors than blood[44–47]. So, how are lymphatic clots initiated? Early studies used chemically-induced damage to vital organs to trigger lymphatic 'thrombosis' in LN sinuses, and found that clots originated from areas of severely damaged endothelium, leading to the speculation that an intact lymphatic endothelium prevents clotting[36]. However, we observed lymphatic clotting even in intact vessels.

NETs are among many factors that help initiate blood coagulation, and have been observed in the lungs and blood of COVID-19 patients[7,8,14]. Inflammatory cytokine-stimulated blood endothelial cells attract neutrophils and can induce NETosis to initiate clot formation[48], so we hypothesized that NETosis may also initiate lymphatic clotting. In response to inflammation or infection, neutrophils are among the first immune cells to reach the LN after encountering virus in the lung; they rapidly enter afferent lymphatics by inducing endothelial junctional retraction[17,23] before entering the LN through the subcapsular sinus[18,20,23,24]. Neutrophil recruitment to the LN is TNFα-dependent[18,19,22,23], which is upregulated and correlated to disease severity in COVID-19[33] and directly stimulates LECs to modulate expression of chemokines, adhesion molecules, and clotting factors[15,49,50]. We found that *in vitro*, TNFα-stimulation of LECs upregulated secretion of CXCL8 and expression of ICAM-1(Fig. S4), both of which are necessary for recruitment of neutrophils to lymphatic vasculature[19,22].

In addition to recruiting neutrophils, CXCL8 also stimulates NETosis[25,26,51]. In blood, DNA and histones in NETs trap platelets to promote clotting[52], but are also sources of tissue

factor[53] and impair protein C activation, so may promote clotting independently of platelets. Inflamed LECs may selectively recruit neutrophils and stimulate NET formation, in turn promoting lymphatic clotting. In our *in vivo* studies, degrading NETs with DNAse 1 injections almost completely eradicated lymphatic clots, indicating that NETosis is a key factor in this pathway.

Interestingly, there is evidence that LN neutrophils in particular can impact adaptive immune responses. Neutrophils, along with macrophages, facilitate antigen capture and presentation in the lymphatic system and carry antigen to the LN[18,22,54]. They can also activate or inhibit T and B cell immunity[18]. Promoting lymphatic clotting through NETosis and therefore impairing antigen and immune cell transport to the LN could be another way neutrophils affect adaptive immunity, and our data showing that serum NET levels negatively correlate with anti-RBD antibody titers indicates that NETs likely do play a role in regulating adaptive immune responses in COVID-19.

Alternatively, lymphatic clotting could play a role in the innate immune response – the primary role of neutrophils is to limit the spread of pathogens throughout the body, and neutrophil depletion can lead to systemic spread of bacterial infection through the lymphatic system[55]. NETosis-induced lymphatic clotting may be another way neutrophils coordinate innate and adaptive immunity by preventing the spread of pathogens throughout the lymphatic system.

Lymphatic vessels are responsible for fluid, solute, and immune cell trafficking to the LN, and GCs require persistent antigen presentation via follicular dendritic cells[56], so it wasn't surprising to find strong correlations between lymphatic clotting and dysfunctional follicles/GCs in the LDLN. Abnormal GC architecture and declining neutralizing antibody titers have been described in a subset of COVID-19 patients[10,27,29,57–60]. While our data only demonstrate a

correlative relationship between clotted LDLN lymphatics and abnormal GC architecture, and NETosis and low anti-RBD antibody titers, one might speculate that blocked lymph flow to and within the LN may impair the progression of adaptive immune responses, although there likely co-exist many contributing mechanisms to GC dysfunction in COVID-19[27]. In future studies it would be important to determine if lymphatic clotting is present in non-lung-draining LNs as well, since dysregulated/missing GCs have been reported in multiple regional LNs in COVID-19[60], but these were not available in this study.

Our findings have both basic and translational relevance to COVID-19. Although lymphatic clots were first observed over a century ago[36,37], the mechanisms by which they form remain elusive. Our data support a new hypothesis that NETosis is a key initiator in lymphatic clotting and highlight the need to further study the consequences of blocked lymph flow in the LN. Translationally, blood coagulopathies, NETosis, and GC dysfunction have all been independently described in COVID-19[5–8,27,28], but our data suggest a new hypothesis that ties them together to suggest therapeutic strategies. Targeting NETs with DNase1 could help restore lymph flow to normalize LN architecture. In conclusion, our data suggest that treatments designed to mitigate TNFα inflammation and degrade NETs may reduce lymphatic clotting and benefit COVID-19 patients.

Acknowledgments

We are thankful to the Human Tissue Resource Center (RRID:SCR_019199), funded by UChicago's Comprehensive Cancer Center Support Grant (P30CA014599), for their assistance with tissue preparation. Whole-slide imaging was performed at the University of Chicago Integrated Light Microscopy Core (RRID:SCR_019197) by Dr. Vytas Bindokas. We also thank

the Regional Organ Bank of Illinois for providing the control lung tissue and Kathy Reilly, Leeon Jones, and Imani Wilson at the Clinical Research Center at the Institute for Translational Medicine for her help with phlebotomy training and whole blood collection for this study. We thank Chaney Giampaolo and Gavin Swartz for their contributions to image analysis. This work was supported by grants from UChicago (UChicago Big Ideas Generator COVID-19 Response Fund, UChicago Women's Board) (M.E.M, M.A.S) and the NIH (grants 1F31CA257763-01 (M.E.M.), 5T32EB009412-12 (T.R.S, G.S.E.) and 5T32AI007090-43 (P.A.S.)), as well as funds kindly donated by Bruce Herzfelder, for which we are extremely grateful. M.E.M., R.K.W., E.C.S., and C.M.S. are PhD candidates at the University of Chicago and this work is submitted in partial fulfillment of the requirement for the PhD.

Authorship

Contributions: MAS, MEM and WWK were responsible for overall study conceptualization and design. AIS, SG, PM, ANH, JM and HS planned and carried out the autopsy tissue collection and pathological analysis, including GC analysis by SG. AIM, AM, CMS, MEM, ECS, RKW, PB, WWK, and MAS conducted experiments and analyzed data. AIS provided control tissue and serum samples. SJR, JY, JT, ARP, and TFG planned and carried out the collection of patient serum samples and clinical data shown in Fig. 6 and 6S. The manuscript was written by MEM, MAS, ECS, CMS, and WWK. MEM and MAS acquired funding for the project and MAS was responsible for overall study supervision.

Conflict-of-interest disclosure: The authors declare no competing financial interests.

Correspondence: Melody A. Swartz, 5640 S. Ellis Ave., ERC 379, University of Chicago, Chicago, IL 60637, melodyswartz@uchicago.edu.

References

1. Dataset. GitHub - CSSEGISandData/COVID-19: Novel Coronavirus (COVID-19) Cases, provided by JHU CSSE. *Dataset COVID-19*. 2020;
2. Elezkurtaj S, Greuel S, Ihlow J, et al. Causes of death and comorbidities in hospitalized patients with COVID-19. *Sci. Rep.* 2021;11(1):.
3. Al-Samkari H, Karp Leaf RS, Dzik WH, et al. COVID-19 and coagulation: Bleeding and thrombotic manifestations of SARS-CoV-2 infection. *Blood*. 2020;136(4):489–500.
4. Tang N, Li D, Wang X, Sun Z. Abnormal coagulation parameters are associated with poor prognosis in patients with novel coronavirus pneumonia. *J. Thromb. Haemost.* 2020;18(4):844–847.
5. Zhou F, Yu T, Du R, et al. Clinical course and risk factors for mortality of adult inpatients with COVID-19 in Wuhan, China: a retrospective cohort study. *Lancet*. 2020;395(10229):1054–1062.
6. Gómez-Mesa JE, Galindo-Coral S, Montes MC, Muñoz Martin AJ. Thrombosis and Coagulopathy in COVID-19. *Curr. Probl. Cardiol.* 2021;46(3):.
7. Veras FP, Pontelli MC, Silva CM, et al. SARS-CoV-2-triggered neutrophil extracellular traps mediate COVID-19 pathology. *J. Exp. Med.* 2020;217(12):.
8. Zuo Y, Yalavarthi S, Shi H, et al. Neutrophil extracellular traps in COVID-19. *JCI Insight*. 2020;5(11):.
9. Liu J, Liu Y, Xiang P, et al. Neutrophil-to-lymphocyte ratio predicts critical illness patients with 2019 coronavirus disease in the early stage. *J. Transl. Med.* 2020;18(1):.
10. Liu J, Li S, Liu J, et al. Longitudinal characteristics of lymphocyte responses and cytokine profiles in the peripheral blood of SARS-CoV-2 infected patients. *EBioMedicine*. 2020;55:.
11. Zuo Y, Yalavarthi S, Shi H, et al. Neutrophil extracellular traps (NETs) as markers of disease severity in COVID-19. *JCI Insight*. 2020;5(11):138999.
12. Varjú I, Kolev K. Networks that stop the flow: A fresh look at fibrin and neutrophil extracellular traps. *Thromb. Res.* 2019;182:1–11.
13. Fuchs TA, Brill A, Wagner DD. Neutrophil extracellular trap (NET) impact on deep vein thrombosis. *Arterioscler. Thromb. Vasc. Biol.* 2012;
14. Middleton EA, He X-Y, Denorme F, et al. Neutrophil Extracellular Traps (NETs) Contribute to Immunothrombosis in COVID-19 Acute Respiratory Distress Syndrome. *Blood*. 2020;
15. G. L, E.J. F, G. C. Hemostatic properties of the lymph: Relationships with occlusion and

thrombosis. *Semin. Thromb. Hemost.* 2012;

16. Kilarski WW, Wachowska M, Muchowicz A, et al. Anti-clotting functions of lymphatics form the natural on-off switch for immune recognition by controlling the antigens and immune cells access to the lymph nodes. *bioRxiv*. 2021;(June):

17. Rigby DA, Ferguson DJP, Johnson LA, Jackson DG. Neutrophils rapidly transit inflamed lymphatic vessel endothelium via integrin-dependent proteolysis and lipoxin-induced junctional retraction. *J. Leukoc. Biol.* 2015;98(6):897–912.

18. Hampton HR, Chtanova T. The lymph node neutrophil. *Semin. Immunol.* 2016;28(2):129–136.

19. Arokiasamy S, Zakian C, Dilliway J, et al. Endogenous TNFα orchestrates the trafficking of neutrophils into and within lymphatic vessels during acute inflammation. *Sci. Rep.* 2017;7:.

20. Takeda A, Hollmén M, Dermadi D, et al. Single-Cell Survey of Human Lymphatics Unveils Marked Endothelial Cell Heterogeneity and Mechanisms of Homing for Neutrophils. *Immunity*. 2019;51(3):561-572.e5.

21. Chakraborty S, Zawieja SD, Wang W, et al. Lipopolysaccharide modulates neutrophil recruitment and macrophage polarization on lymphatic vessels and impairs lymphatic function in rat mesentery. *Am. J. Physiol. - Hear. Circ. Physiol.* 2015;309(12):H2042–H2057.

22. Stephens M, Liao S. Neutrophil–lymphatic interactions during acute and chronic disease. *Cell Tissue Res.* 2018;371(3):599–606.

23. Schineis P, Runge P, Halin C. Cellular traffic through afferent lymphatic vessels. *Vascul. Pharmacol.* 2019;112:31–41.

24. Gorlino C V., Ranocchia RP, Harman MF, et al. Neutrophils Exhibit Differential Requirements for Homing Molecules in Their Lymphatic and Blood Trafficking into Draining Lymph Nodes. *J. Immunol.* 2014;193(4):1966–1974.

25. Nie M, Yang L, Bi X, et al. Neutrophil Extracellular Traps Induced by IL8 Promote Diffuse Large B-cell Lymphoma Progression via the TLR9 Signaling. *Clin. Cancer Res.* 2019;25(6):1867–1879.

26. Gonzalez-Aparicio M, Alfaro C. Influence of interleukin-8 and neutrophil extracellular trap (NET) formation in the tumor microenvironment: Is there a pathogenic role? *J. Immunol. Res.* 2019;2019:.

27. Kaneko N, Kuo H-H, Boucau J, et al. Loss of Bcl-6-expressing T follicular helper cells and germinal centers in COVID-19. *Cell*. 2020;

28. Woodruff MC, Ramonell RP, Nguyen DC, et al. Extrafollicular B cell responses correlate with neutralizing antibodies and morbidity in COVID-19. *Nat. Immunol.* 2020;21(12):1506–1516.

29. Sette A, Crotty S. Adaptive immunity to SARS-CoV-2 and COVID-19. *Cell*. 2021;184(4):861–880.

30. Iwen PC, Stiles KL, Pentella MA. Safety Considerations in the Laboratory Testing of Specimens Suspected or Known to Contain the Severe Acute Respiratory Syndrome Coronavirus 2 (SARS-CoV-2). *Am. J. Clin. Pathol.* 2020;153(5):567–570.

31. Gajewski T, Rouhani S, Trujillo J, et al. Severe COVID-19 infection is associated with aberrant cytokine production by infected lung epithelial cells rather than by systemic immune dysfunction. *Res. Sq.* 2021;

32. Güç E, Fankhauser M, Lund AW, Swartz MA, Kilarski WW. Long-term intravital immunofluorescence imaging of tissue matrix components with epifluorescence and two-photon microscopy. *J. Vis. Exp.* 2014;(86):.

33. Costela-Ruiz VJ, Illescas-Montes R, Puerta-Puerta JM, Ruiz C, Melguizo-Rodríguez L. SARS-CoV-2 infection: The role of cytokines in COVID-19 disease. *Cytokine Growth Factor Rev.* 2020;54:62–75.

34. Kirchhofer D, Tschopp TB, Hadvary P, Baumgartner HR. Endothelial cells stimulated with tumor necrosis factor-α express varying amounts of tissue factor resulting in inhomogenous fibrin deposition in a native blood flow system. Effects of thrombin inhibitors. *J. Clin. Invest.* 1994;93(5):2073–2083.

35. Pircher J, Merkle M, Wörnle M, et al. Prothrombotic effects of tumor necrosis factor alpha in vivo are amplified by the absence of TNF-alpha receptor subtype 1 and require TNF-alpha receptor subtype 2. *Arthritis Res. Ther.* 2012;14(5):.

36. Opie EL. Lymph formation and edema of the liver with experimental nephritis produced by cantharidin. *J. Exp. Med.* 1912;16(6):831–849.

37. Opie EL. Thrombosis and Occlusion of Lymphatics. *J. Med. Res.* 1913;

38. Howell WH. THE COAGULATION OF LYMPH. *Am. J. Physiol. Content*. 1914;35(4):483–491.

39. Case T, Leis B, Witte M, et al. Vascular abnormalities in experimental and human lymphatic filariasis. *Lymphology*. 1991;24(4):174–183.

40. Hara H, Mihara M, Ohtomo R, Tanaka S. Lymphatic Vessel Thrombosis in a Patient with Secondary Lymphedema. *Plast. Reconstr. Surg. - Glob. Open*. 2019;7(5):e2268.

41. Hara H, Mihara M, Anan T, et al. Pathological Investigation of Acquired Lymphangiectasia Accompanied by Lower Limb Lymphedema: Lymphocyte Infiltration in the Dermis and Epidermis. *Lymphat. Res. Biol.* 2016;14(3):172–180.

42. Hara H, Mihara M, Seki Y, Koshima I. Lymphoedema caused by idiopathic lymphatic thrombus. *J. Plast. Reconstr. Aesthetic Surg.* 2013;66(12):1780–1783.

43. Fader RC, Ewert A. Evolution of lymph thrombi in experimental Brugia malayi infections: A scanning electron microscopic study. *Lymphology*. 1986;19(4):146–152.

44. Brinkhous KM, Walker SA. PROTHROMBIN AND FIBRINOGEN IN LYMPH. *Am. J. Physiol.*

Content. 1941;132(3):666–669.

45. Le DT, Borgs P, Toneff TW, Witte MH, Rapaport SI. Hemostatic factors in rabbit limb lymph: Relationship to mechanisms regulating extravascular coagulation. *Am. J. Physiol. - Hear. Circ. Physiol.* 1998;274(3 43-3):.

46. Menkin V. Studies on inflammation. *J. Exp. Med.* 1936;64(3):485–502.

47. Fantl P, Nelson JF. Coagulation in lymph. *J. Physiol.* 1953;122(1):33–37.

48. Gupta AK, Joshi MB, Philippova M, et al. Activated endothelial cells induce neutrophil extracellular traps and are susceptible to NETosis-mediated cell death. *FEBS Lett.* 2010;584(14):3193–3197.

49. Laschinger CA, Johnston MG, Hay JB, Wasi S. Production of plasminogen activator and plasminogen activator inhibitor by bovine lymphatic endothelial cells: Modulation by TNF-α. *Thromb. Res.* 1990;59(3):567–579.

50. Liu Y, Pelekanakis K, Woolkalis MJ. Thrombin and tumor necrosis factor α synergistically stimulate tissue factor expression in human endothelial cells: Regulation through c-Fos and c-Jun. *J. Biol. Chem.* 2004;279(34):36142–36147.

51. Lee KH, Kronbichler A, Park DDY, et al. Neutrophil extracellular traps (NETs) in autoimmune diseases: A comprehensive review. *Autoimmun. Rev.* 2017;16(11):1160–1173.

52. Fuchs TA, Brill A, Duerschmied D, et al. Extracellular DNA traps promote thrombosis. *Proc. Natl. Acad. Sci. U. S. A.* 2010;107(36):15880–15885.

53. Stakos DA, Kambas K, Konstantinidis T, et al. Expression of functional tissue factor by neutrophil extracellular traps in culprit artery of acute myocardial infarction. *Eur. Heart J.* 2015;36(22):1405–1414.

54. Lok LSC, Dennison TW, Mahbubani KM, et al. Phenotypically distinct neutrophils patrol uninfected human and mouse lymph nodes. *Proc. Natl. Acad. Sci. U. S. A.* 2019;116(38):19083–19089.

55. Kastenmüller W, Torabi-Parizi P, Subramanian N, Lämmermann T, Germain RN. A spatially-organized multicellular innate immune response in lymph nodes limits systemic pathogen spread. *Cell*. 2012;150(6):1235–1248.

56. Kranich J, Krautler N. How follicular dendritic cells shape the B-cell antigenome. *Front. Immunol.* 2016;7(JUN):

57. Lucas C, Wong P, Klein J, et al. Longitudinal analyses reveal immunological misfiring in severe COVID-19. *Nature*. 2020;584(7821):463–469.

58. Robbiani DF, Gaebler C, Muecksch F, et al. Convergent antibody responses to SARS-CoV-2 in convalescent individuals. *Nature*. 2020;584(7821):437–442.

59. Long QX, Liu BZ, Deng HJ, et al. Antibody responses to SARS-CoV-2 in patients with COVID-19. *Nat. Med.* 2020;26(6):845–848.

60. Haslbauer JD, Matter MS, Stalder AK, Tzankov A. Histomorphological patterns of regional lymph nodes in COVID-19 lungs. *Pathologe*. 2021;42(S1):.

Fig. 1. Fibrin clots in lymphatic vessels in lungs of COVID-19 decedents. Representative immunofluorescence images of lung sections showing fibrin (green) and podoplanin$^+$ lymphatic endothelial cells (red) with 488 autofluorescence (gray) to show tissue structure. Yellow arrows indicate clotted lymphatic vessels and white arrows indicate damaged lymphatic endothelium. Scale bars = 100 μm.

Fig. 2. Lymphatic clotting is widespread in lung-draining lymph nodes of COVID-19 decedents. (A) Representative immunofluorescence image showing a large lymphatic clot in a lung-draining LN (LDLN) section with fibrin (green) and podoplanin (red), with inset **(A(i))** highlighting the fibrillar structure of the fibrin clot in 488 autofluorescence (gray)). **(B-D)** Representative images showing intralymphatic fibrin clots in LDLNs of (B) COVID-19 decedents, **(C)** control decedents without viral infections, and **(D)** H1N1 decedents, with arrows indicating partially or fully clotted vessels and arrowheads indicating open vessels. Scale bars in **A-D** = 100 μm. **(E)** Lymphatic clotting score rubric showing examples for each score. 0: no fibrin (fully open), 1: fibrin confined to endothelium, 2: minimal intralymphatic fibrin (<20% of vessel lumen), 3: partially occluded (>20% of lumen), 4: fully occluded. **(F)** Percentage of clotted lymphatic vessels (with a fibrin score of 3-4) in LDLNs from COVID-19, control, and H1N1 decedents; each dot shows the average from 3 sections of each patient. (**G**) Average lymphatic fibrin score in each LDLN. Bars in **F-G** represent median ± 95% confidence interval; *p < 0.05, **p < 0.01 by one-way ANOVA with Tukey multiple comparisons post-test.

Fig. 3: Abnormal germinal center architecture in LDLNs of COVID-19 decedents correlates with lymphatic clotting in LDLN. (A-D) Representative images from stained LDLNs comparing features of normal (left), regressed (middle), and otherwise abnormal (right) germinal center (GC) follicles of COVID-19 and control decedents. **(A)** H&E-stained tiled images where the abnormal (right) lacks secondary follicle formation altogether. **(B)** Zoomed-in H&E-stained images showing (left) a normal secondary follicle, (middle) a regressed follicle lacking a mantle zone and containing TBMs (black arrows), and (right) complete lack of follicle architecture. (**C**) Representative immunofluorescence images showing lymphocyte activation in control (**left**) and COVID-19 (**middle, right**) LDLNs; CD83 (cyan), GL7 (red) and CD20 (green). (**Left**) shows strong follicle formation and activation, (**middle)** shows decreased follicle size and density, and (**right**) shows abnormal follicle structure and extensive extrafollicular activation. (**D**) Representative immunofluorescence images of T (CD3, red) and B cell (CD20, green) zone integrity in COVID-19 LDLNs. (**Left**) shows dense B cells and distinct T/B separation, while (**middle**) shows decreased follicle size and density, and (**right**) shows decreased cellularity and poor T/B zone integrity. (**E**) Average GC abnormality scores for LDLNs of COVID-19, H1N1 and control decedents. Dashed line represents the median for each group and dotted lines represent the first and third quartiles. ***p < 0.001, one-way ANOVA test with Tukey multiple comparisons test. (**F**) Linear regression correlations of GC abnormality score vs. % clotted lymphatic vessels in LDLNs from COVID-19 (black), H1N1 (blue), and control (red) decedents. Scale bars in **A,** 500 μm; **B-D**, 100 μm.

Fig. 4: Lymph clotting in LDLNs correlates with intralymphatic NETs in the LDLN and neutrophil load in the lungs of COVID-19 decedents. (A) Representative tiled immunofluorescence image of COVID-19 LDLN showing NETs (H3cit, red) integrated into fibrin clots (green) within a large lymphatic vessel (PDPN, blue) near the subcapsular sinus. **(B)** Percentage of clotted (fibrin score 3-4) or open (fibrin score 0-2) lymphatic vessels that contain

NETs in LDLNs from control (red), COVID-19 (black), and H1N1 (blue) decedents. Dashed line represents the median for each group and dotted lines represent the first and third quartiles. **p < 0.01 by two-tailed paired Student's t-test. **(C-D)** Correlation of average NET score (rubric shown Fig. S3) with % clotted lymphatic vessels (**C**) and GC abnormality score (**D**) in each LDLN. **(E)** Representative tiled immunofluorescence images from lung (left) and matching LDLN (right) from two different COVID-19 patients showing relationship between neutrophil density in the lung with lymphatic clotting and intralymphatic NETs in the LDLN. In Patient A (top), a low density of neutrophils and NETs (MPO, yellow; H3cit, red) in the lung (left) corresponded to a LDLN (right) with mostly open lymphatic vessels (fibrin, green; PDPN, blue; H3cit, red); while in Patient B (bottom), high levels of neutrophils in the lung corresponded to extensive intralymphatic fibrin clots and high levels of intralymphatic NETs in the LDLNs. (**E-F**) The density of neutrophils in the lungs correlates with lymphatic clotting in the LDLN of COVID-19 decedents. Linear regression correlations of **(F)** % clotted LDLN lymphatic vessels (fibrin score 3-4) vs. lung neutrophil density and **(G)** % clotted LDLN lymphatic vessels vs. lung NETs density. Scale bars in **A, E** = 100 μm.

Fig. 5: In serum from hospitalized COVID-19 patients, levels of NET markers did not correlate with disease severity or d-dimer levels but did correlate with lower anti-RBD antibody titers. (A) Serum levels of MPO-DNA from hospitalized COVID-19 and control patients, normalized to NET-standard. **(B)** Scatter plot of D-dimer vs. MPO-DNA levels in patient serum showing no correlation between the two ($R^2 = 0.0217$, $p = 0.29$ from linear regression analysis). Dotted horizontal lines indicate low (<0.5 μg/ml FEU), mid (between 0.5 and 2 μg/mL FEU) and high (> 2 μg/mL FEU) D-dimer levels. Dotted vertical lines indicate low (<0.33), mid (0.33-0.5) and high (>0.5) levels of MPO-DNA. Dot colors indicate patients with low (red), mid (orange) or high (green) anti-RBD titers. **(C)** Scatter plot of anti-RBD antibody titers vs MPO-DNA levels in patient serum ($R^2 = 0.1487$, $p = 0.0043$ from linear regression analysis). Dotted horizontal lines indicate low (≤4), mid (4.5-5.5), and high (≥6) anti-RBD antibody titers and dotted vertical lines are as in **(B)**. Dot colors indicate patients with high (red), mid (orange) or low (green) levels of D-dimer. **(D)** Average MPO-DNA levels from patients with low (2-4), mid (4.5-5.5), or high (6-8) titers of anti-RBD antibodies. **(E)** Proportion of patients in each anti-RBD titer group (low, mid or high) that had low, mid, or high MPO-DNA levels. **(F)** Average anti-RBD titers from patients with low (<0.33), mid (0.33-0.5) or high (>0.5) MPO-DNA levels. **(G)** Proportion of patients in each MPO-DNA group (low, mid or high) that had low, mid or high anti-RBD titers. In (**A,D,F**), dashed line represents the median for each group and dotted lines represent the first and third quartiles. In (**A**), **p < 0.01 by unpaired two-tailed t-test and in (**D,F**), *p < 0.05, **p < 0.01 by one-way ANOVA test with Tukey's multiple comparisons test.

Fig. 6: Local injection of TNFα or inactivated thrombin induces NET-dependent intralymphatic fibrin coagulation and blocks lymphatic drainage in mouse skin. (A) Representative immunofluorescence images of thrombomodulin (thrmod, red), CD31 (green), tissue factor (TF, green), and von Willebrand factor (von Willnbrd, red) staining in mouse ears. Arrows point to collecting lymphatics that contain unique morphological features (i.e., valves with uneven vessel diameters). **Left:** Thrombomodulin expression overlaps with CD31 and is also present in some interstitial and perivascular cells and nerve fibers (n). **Middle**: Both blood and lymphatic vessels express thrombomodulin, but only blood vessels express tissue factor.

Tissue factor expression in lymphatics is limited to perivascular cells and adipocytes (a). **Right**: In contrast to blood vessels, lymphatic vessels did not express von Willebrand factor. Scale bars = 50 μm. **(B)** Schematic of experimental design: Intradermal injection of clot initiators (CIs) TNFα**,** TNFα and IL-1β, or inactivated thrombin, on day 0 was followed by intravenous injection of FITC-labeled fibrinogen 30 min later. 6h after the first injection, the procedure was repeated. The mice were perfused and fixed after 20h. **(C)** Representative confocal whole-mount images of lymphatic collectors occluded by fibrin (green) clots after treatment with TNFα (**left**), TNFα and IL-1β, (**middle**), or inactivated thrombin (**right**). Basement membrane (BM, gray) is represented by collagen-IV staining. Scale bars = 50 μm. **(D)** Schematic of experimental design: Intradermal injection of clot initiator (TNFα) and intraperitoneal injection of DNAse 1 on day 0 was followed by intravenous injection of 647-labeled fibrinogen 30 minutes later. 6h after the first injection the procedure was repeated, and the mice were perfused and fixed after 20h. Control mice received TNFα but not DNAse 1 injections. **(E)** Representative whole-mount immunofluorescence staining images of lymphatic vessels and clots in the mouse ear in control mice (left) and mice that received DNAse 1 injections (right) (LYVE-1, white; H3cit, red; fibrinogen, green). White arrows indicate lymphatic clots (left inset: LYVE-1 and H3cit channels of clot containing NETs, right inset: LYVE-1 and H3cit channels of clot outside of a lymphatic with no NETs) and yellow arrows indicate clots outside of lymphatics, likely in a blood vessel. Scale bar = 100 μm. **(F)** Averaged number of lymphatic clots in the left and right ear dorsal dermis for each mouse injected i.d. with TNFα (n=5) and each mouse injected with both TNFα and DNAse-1 (n=5). Bars and error bars represent median and 95% confidence interval. ***p < 0.001 by unpaired two-tailed t-test.

Figure 1

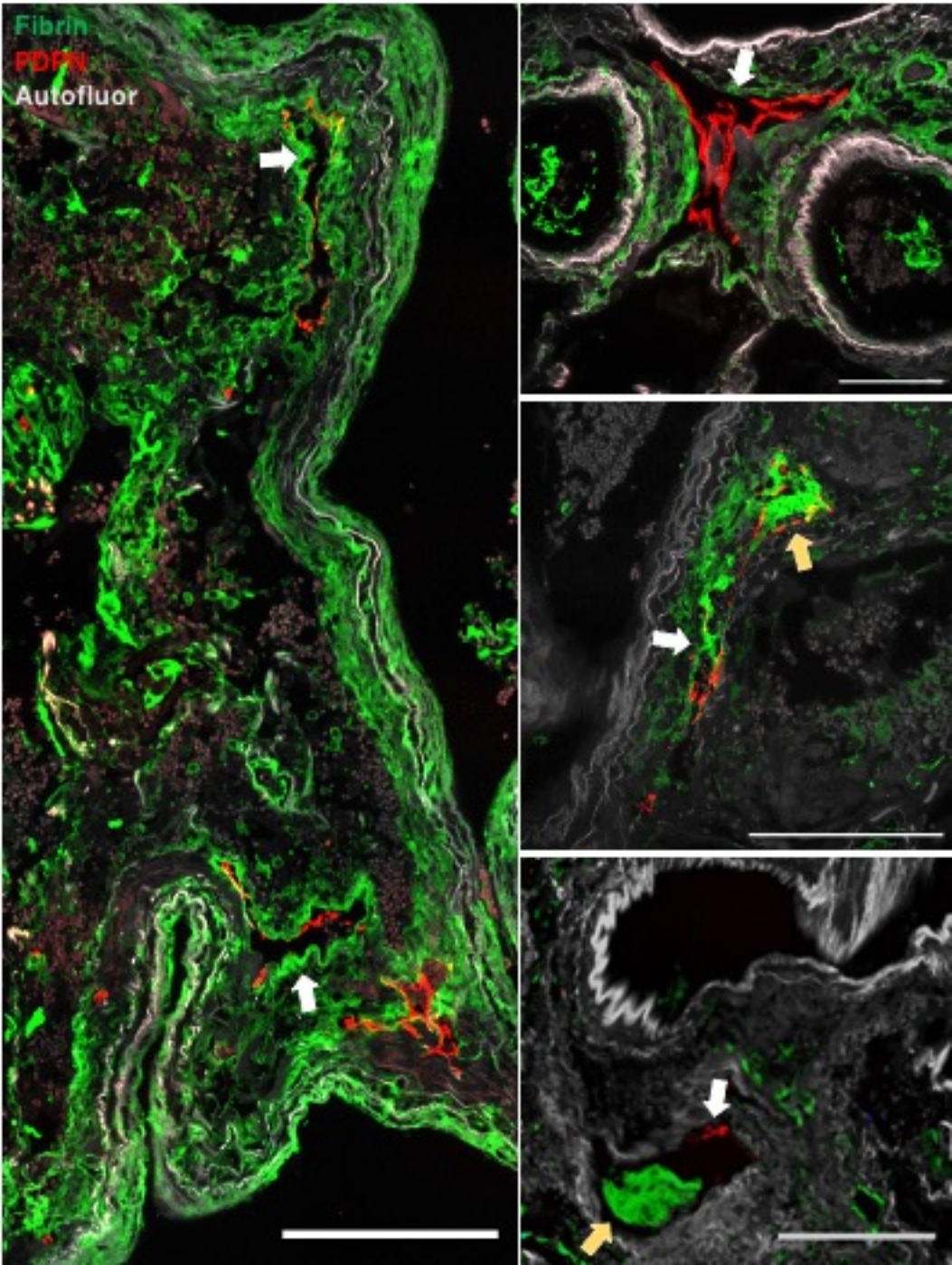

Figure 2

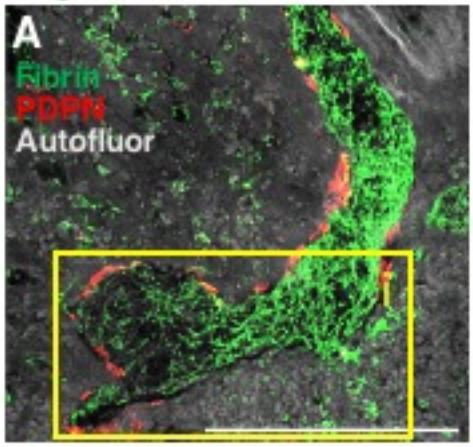
A
Fibrin
PDPN
Autofluor

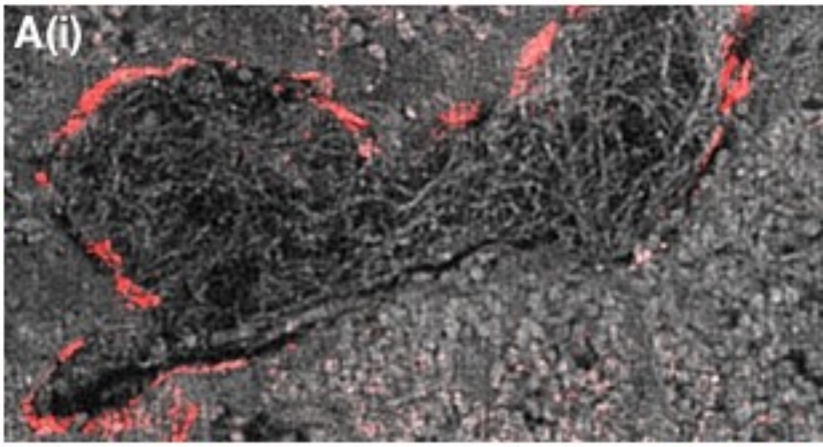
A(i)

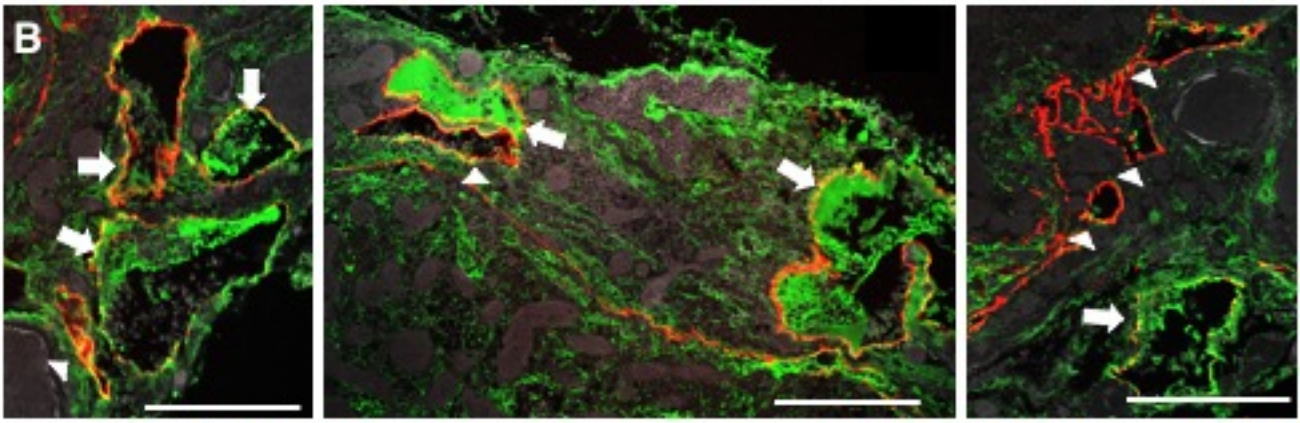
B

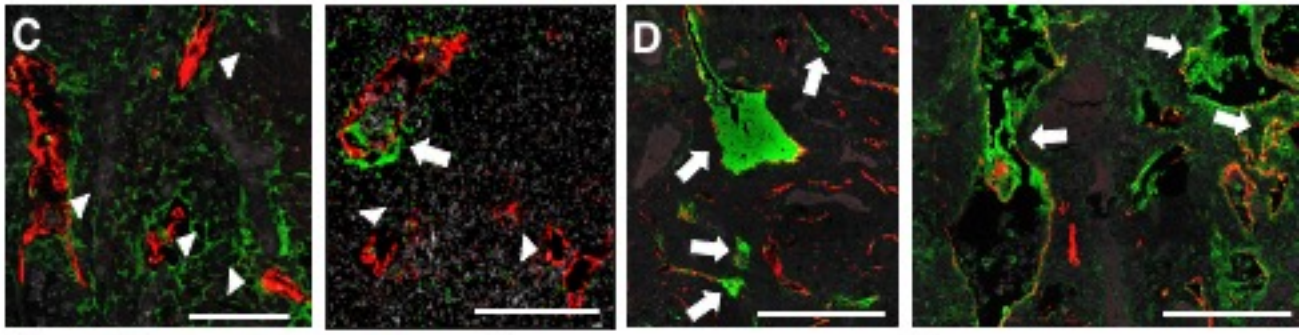
C
D

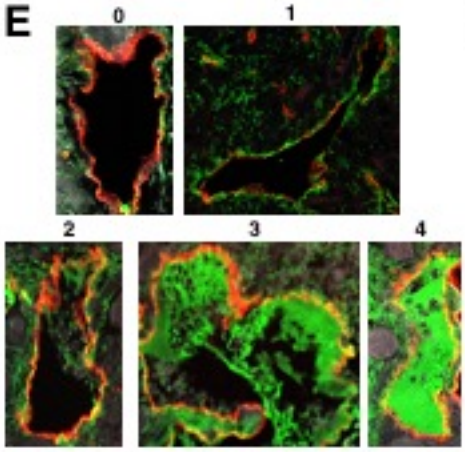
E
0
1
2
3
4

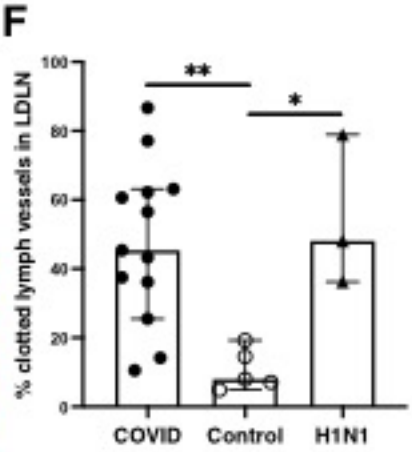
F
% clotted lymph vessels in LDLN
100
80
60
40
20
0
**
*
COVID
Control
H1N1

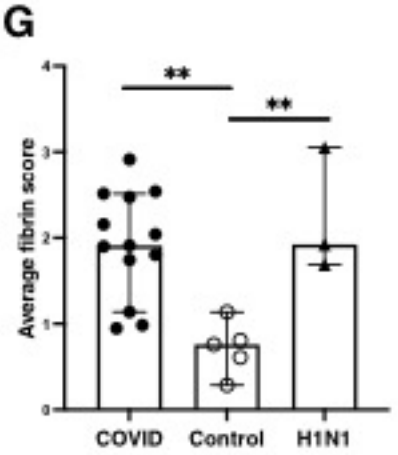
G
Average fibrin score
4
3
2
1
0
**
**
COVID
Control
H1N1

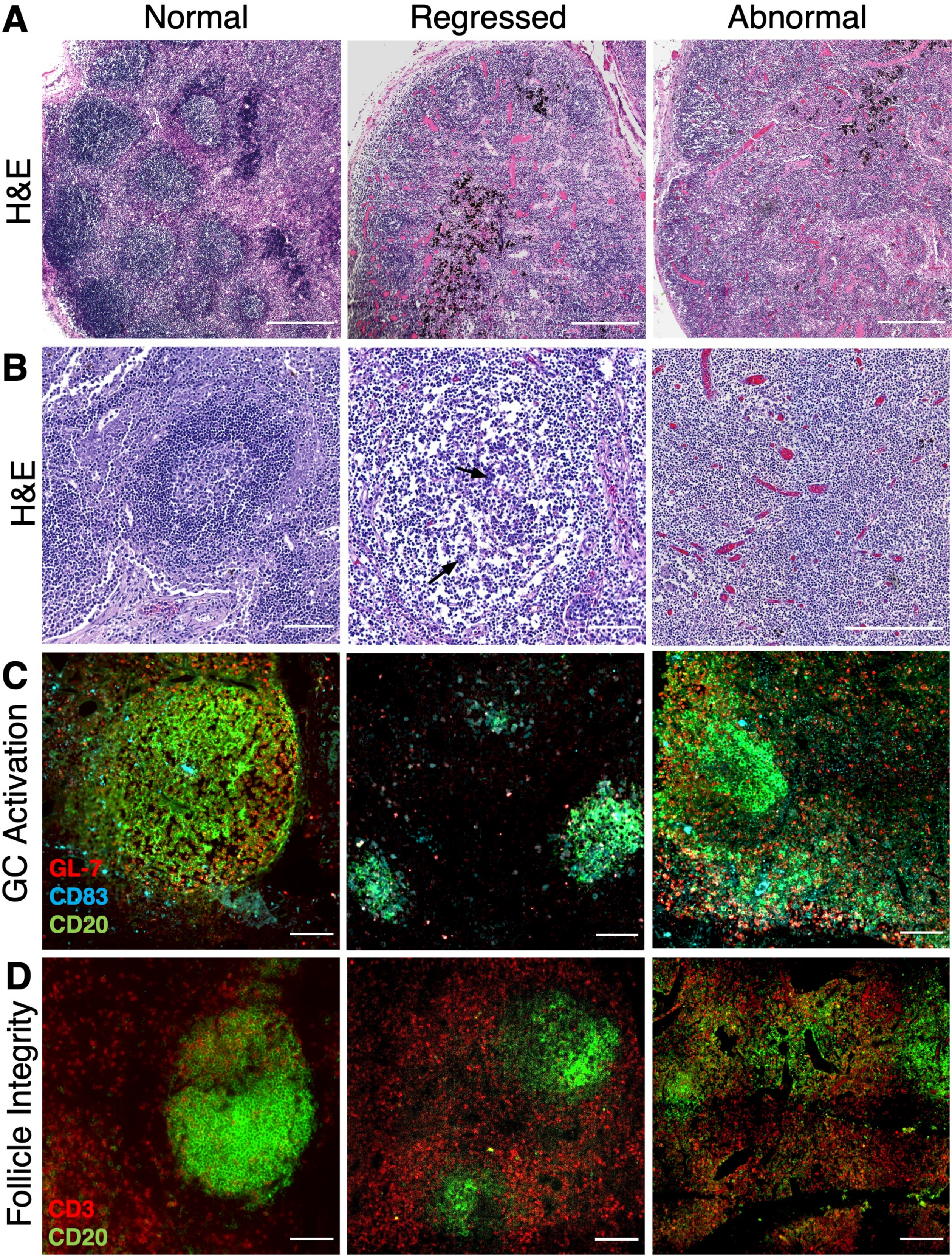
A
Normal
Regressed
Abnormal
H&E
B
H&E
C
GC Activation
GL-7
CD83
CD20
D
Follicle Integrity
CD3
CD20
E
***
ns
*
GC score
20
15
10
5
0
COVID-19
H1N1
Control
F
GC score
20
15
10
5
0
0
20
40
60
80
100
% clotted lymph vessels
R2=0.33
p=0.006

Figure 4

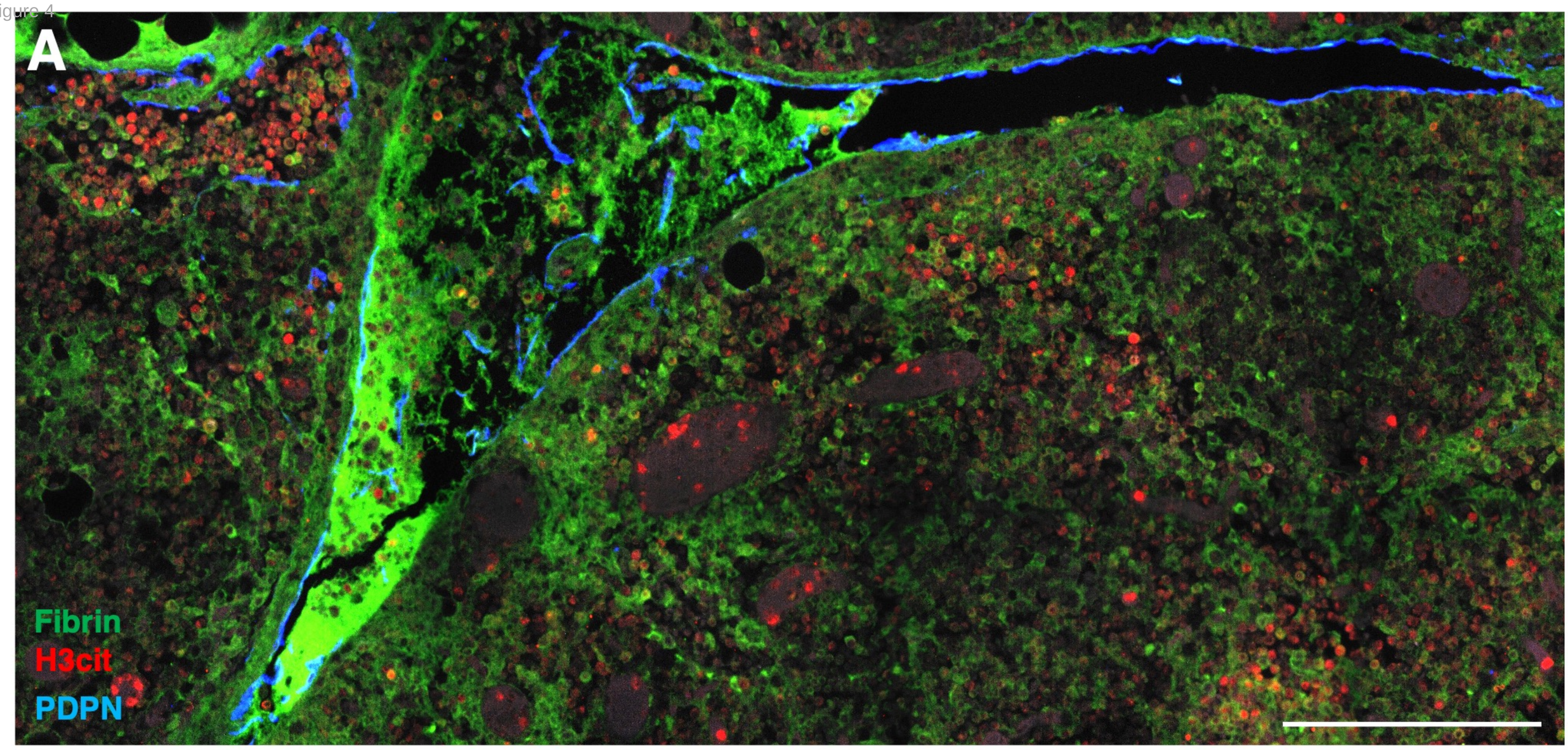
A
Fibrin
H3cit
PDPN

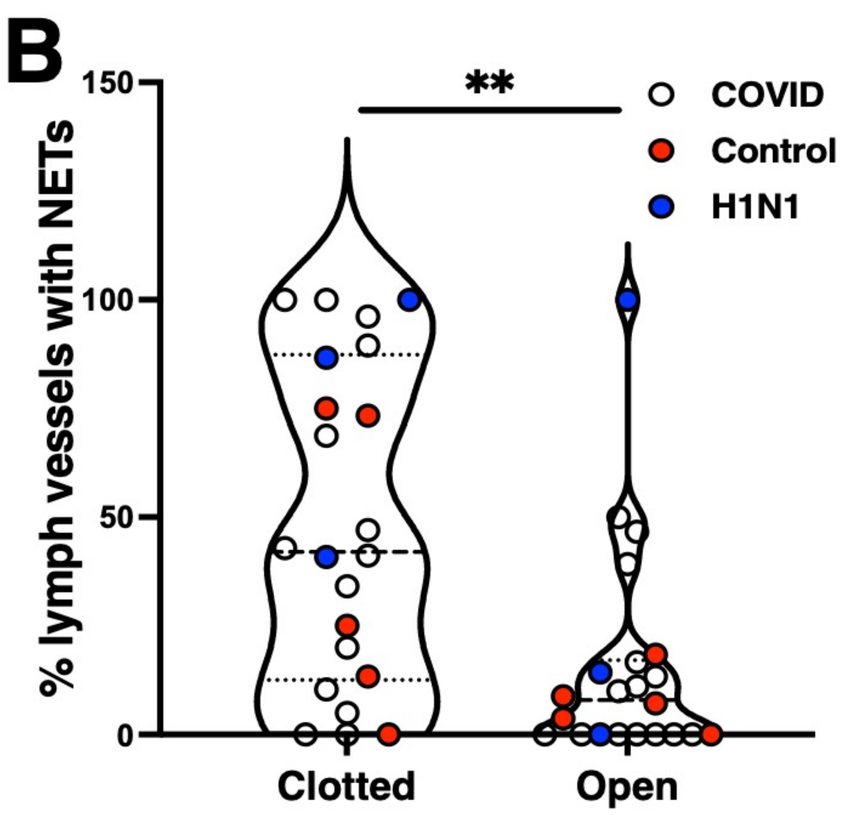
B
**
COVID
Control
H1N1
% lymph vessels with NETs
150
100
50
0
Clotted
Open

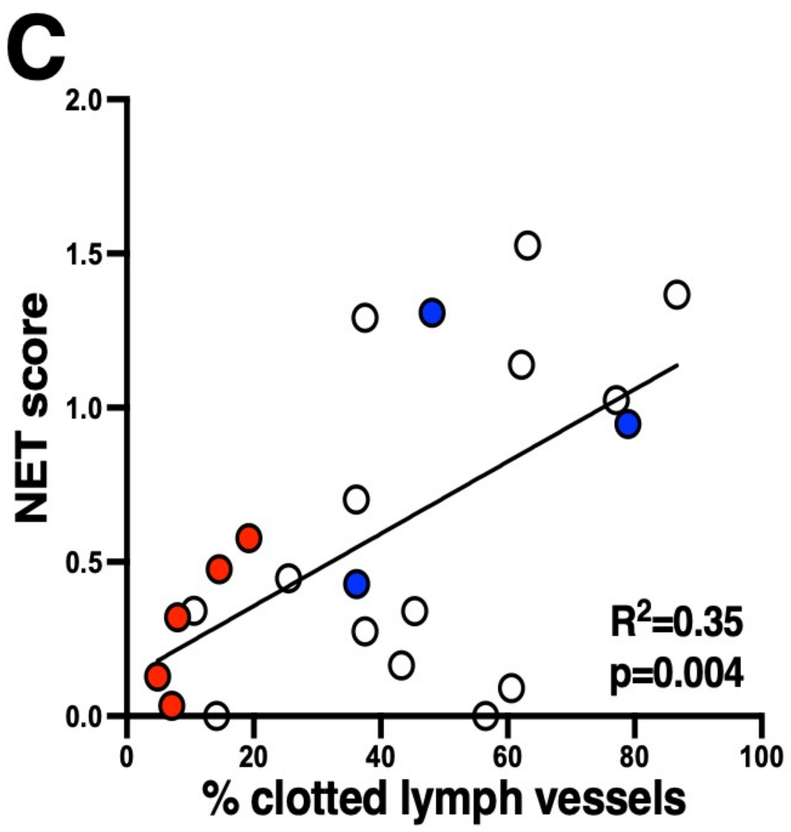
C
NET score
2.0
1.5
1.0
0.5
0.0
R2=0.35
p=0.004
0
20
40
60
80
100
% clotted lymph vessels

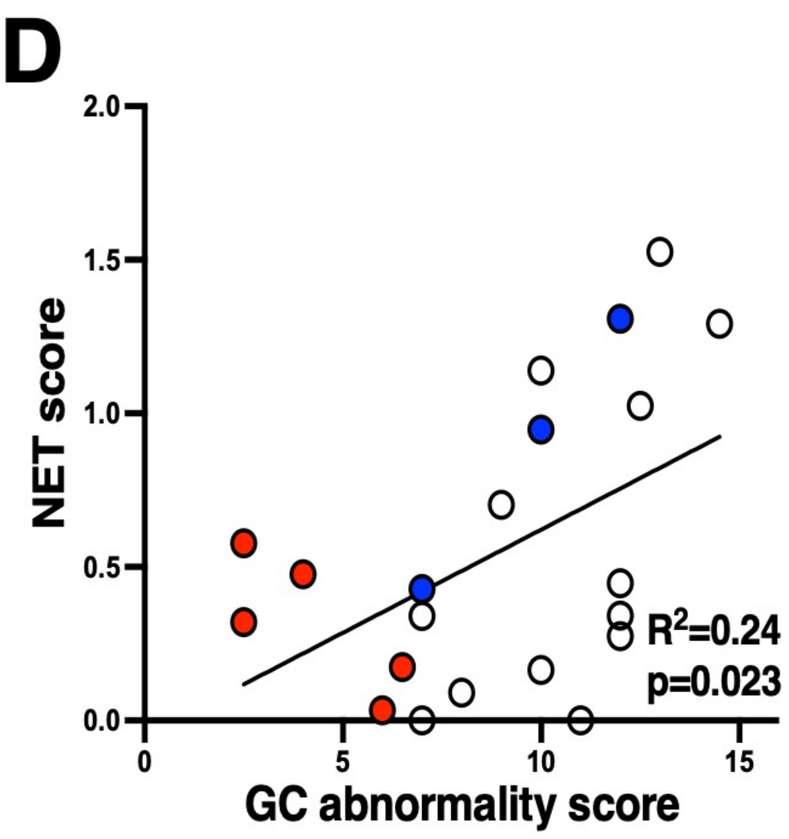
D
NET score
2.0
1.5
1.0
0.5
0.0
R2=0.24
p=0.023
0
5
10
15
GC abnormality score

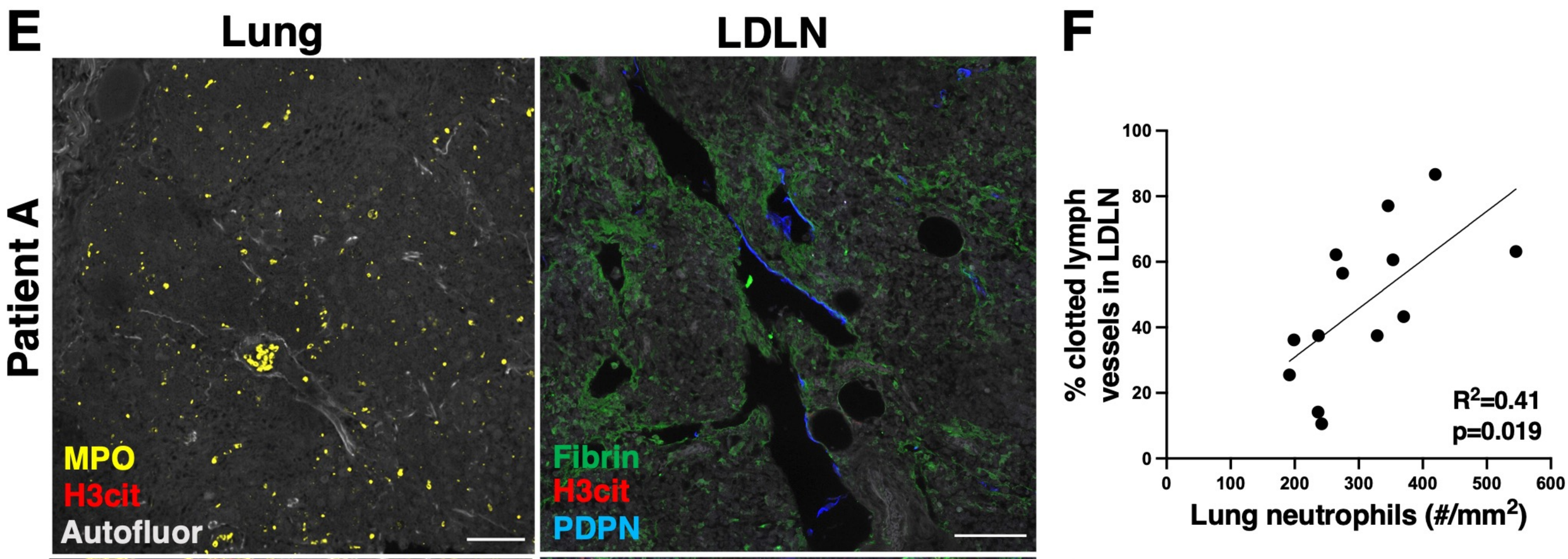
E
Lung
LDLN
Patient A
MPO
H3cit
Autofluor
Fibrin
H3cit
PDPN
F
% clotted lymph vessels in LDLN
100
80
60
40
20
0
R2=0.41
p=0.019
0
100
200
300
400
500
600
Lung neutrophils (#/mm2)

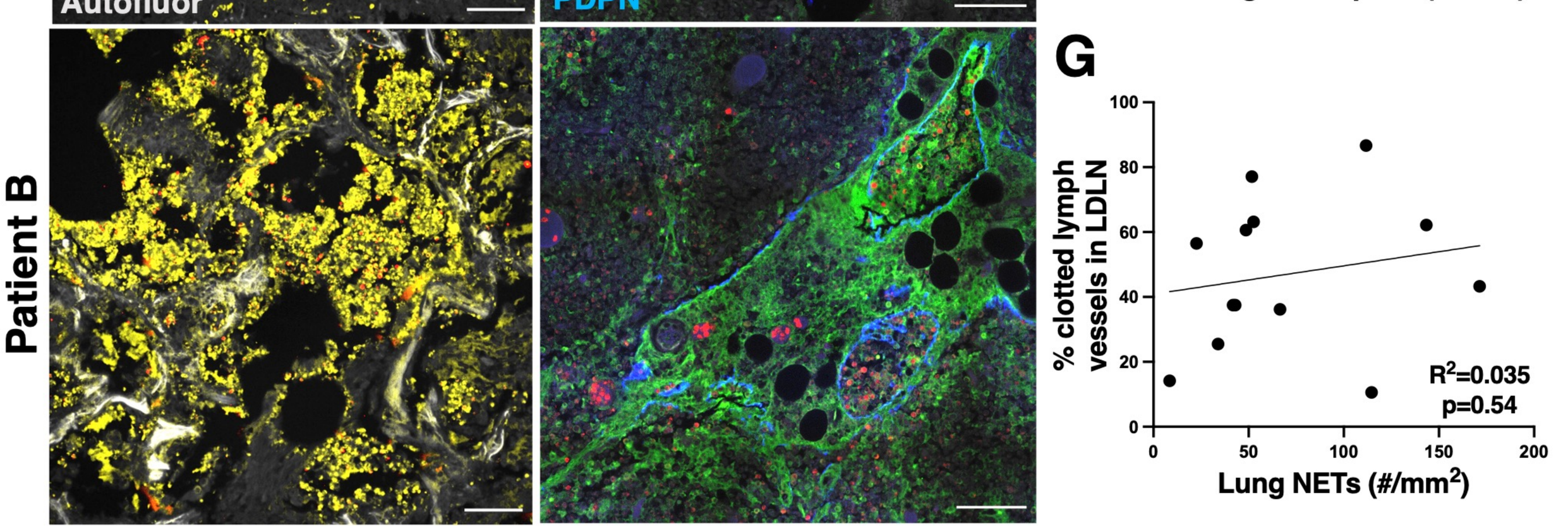
Patient B
G
% clotted lymph vessels in LDLN
100
80
60
40
20
0
R2=0.035
p=0.54
0
50
100
150
200
Lung NETs (#/mm2)

Figure 5

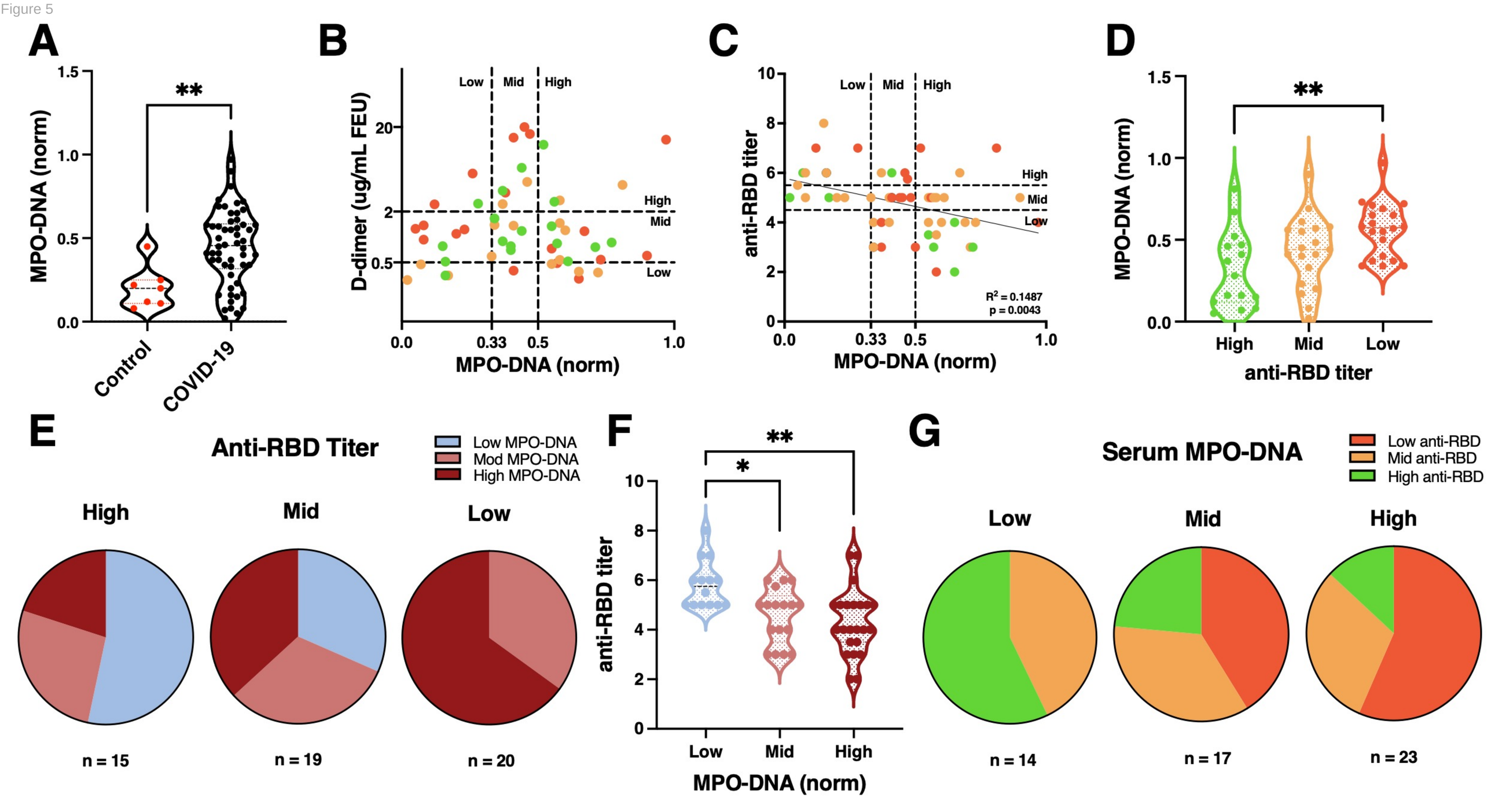
A
MPO-DNA (norm)
1.5
1.0
0.5
0.0
**
Control
COVID-19
B
D-dimer (ug/mL FEU)
20
2
0.5
Low
Mid
High
High
Mid
Low
0.0
0.33
0.5
1.0
MPO-DNA (norm)
C
anti-RBD titer
10
8
6
4
2
0
Low
Mid
High
High
Mid
Low
R² = 0.1487
p = 0.0043
0.0
0.33
0.5
1.0
MPO-DNA (norm)
D
MPO-DNA (norm)
1.5
1.0
0.5
0.0
**
High
Mid
Low
anti-RBD titer
E
Anti-RBD Titer
Low MPO-DNA
Mod MPO-DNA
High MPO-DNA
High
Mid
Low
n = 15
n = 19
n = 20
F
**
*
anti-RBD titer
10
8
6
4
2
0
Low
Mid
High
MPO-DNA (norm)
G
Serum MPO-DNA
Low anti-RBD
Mid anti-RBD
High anti-RBD
Low
Mid
High
n = 14
n = 17
n = 23

Figure 6

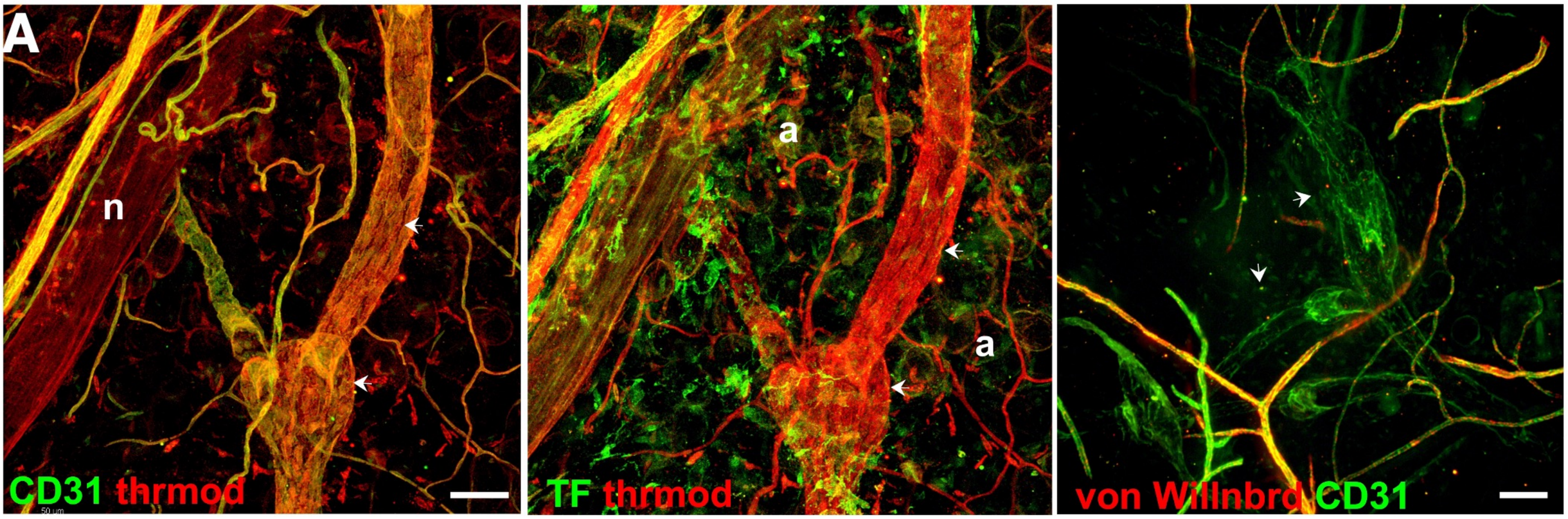
A
n
a
a
CD31 thrmod
TF thrmod
von Willnbrd CD31


B
0
30 min
6h
6h 30 min
20h
i.d. Cl
i.v. FITC-fibrinogen
i.d. Cl
i.v. FITC-fibrinogen
Image, perfuse & fix

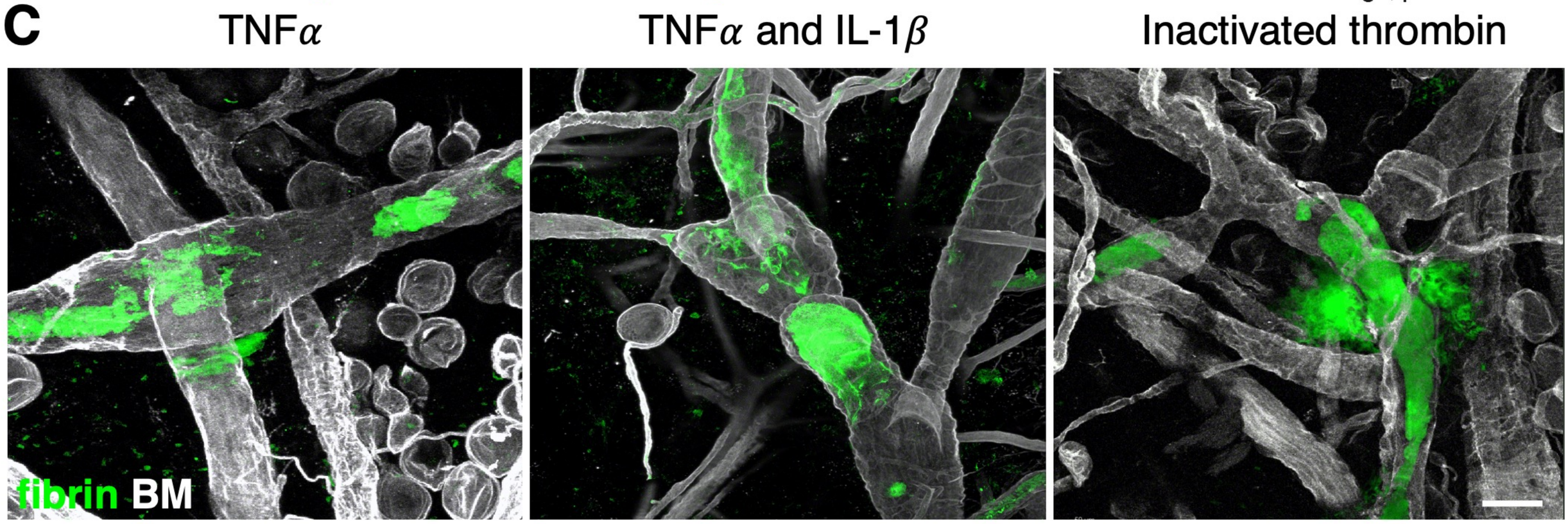
C
TNFα
TNFα and IL-1β
Inactivated thrombin
fibrin BM


D
0
30 min
6h
6h 30 min
20h
i.d. Cl
i.p. DNAse 1
i.v. 647-fibrinogen
i.d. Cl
i.p. DNAse 1
i.v. 647-fibrinogen
Image, perfuse & fix

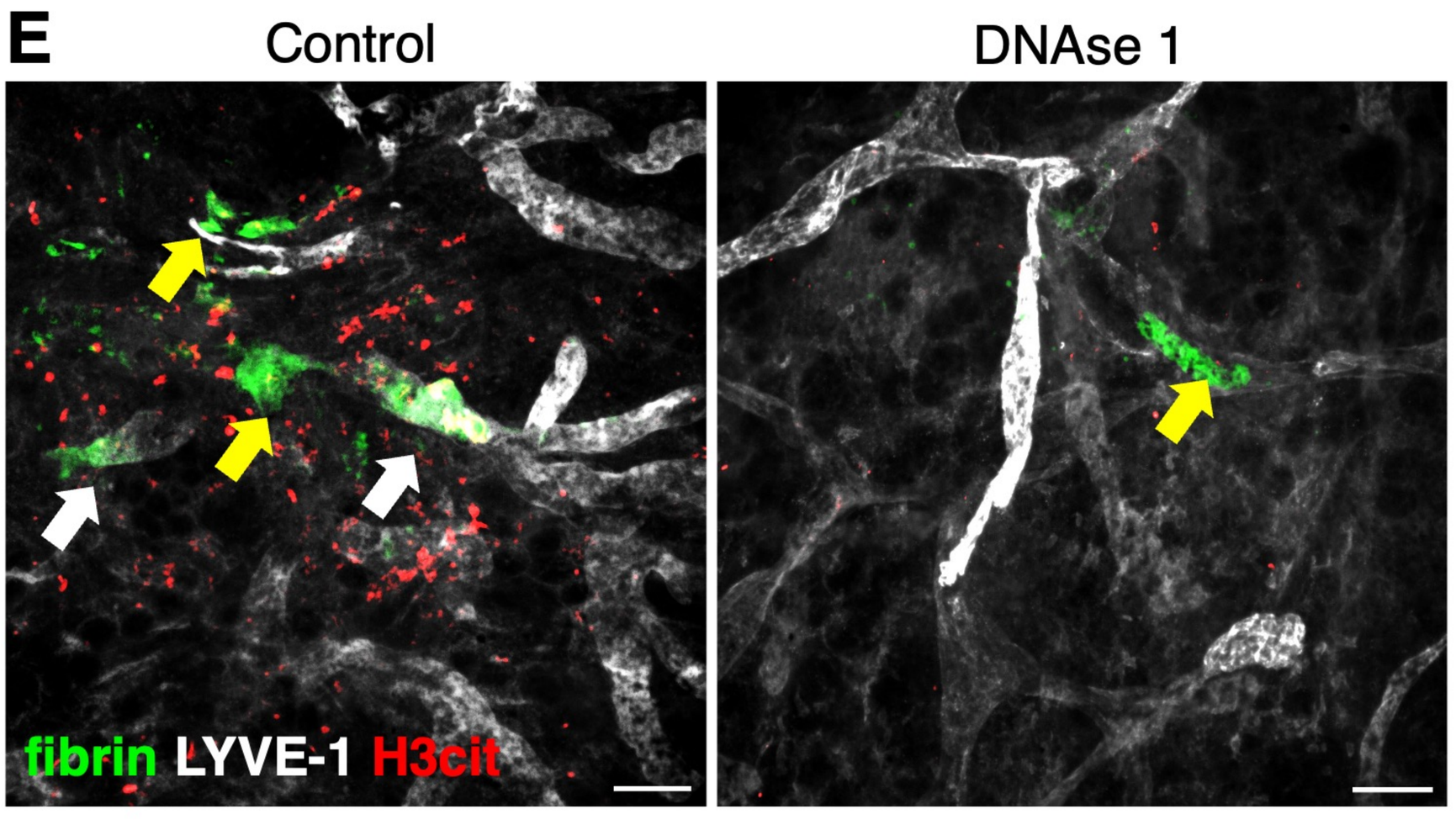
E
Control
DNAse 1
fibrin LYVE-1 H3cit

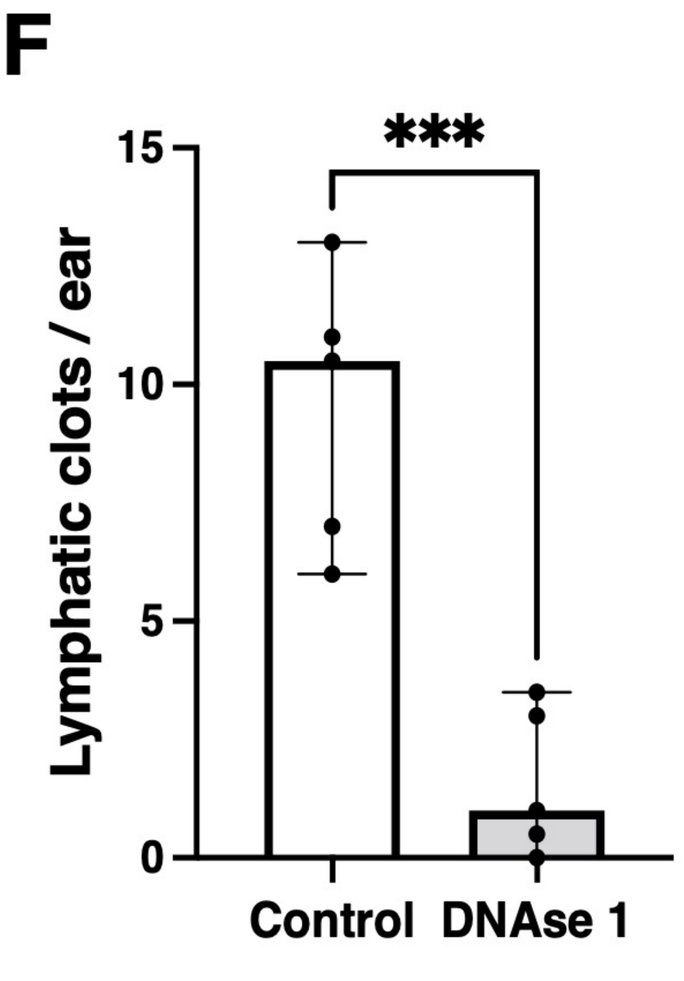
F
***
15
10
5
0
Lymphatic clots / ear
Control
DNAse 1